Semiconductor Physics, Quantum Electronics & Optoelectronics, 2013. V. 16, N 3. P. 265-272.

PACS 61.05.cp, 61.72.uj, 68.65.-k

X-ray diffraction investigation of GaN layers on Si(111) and Al_2O_3 (0001) substrates

N.V. Safriuk, G.V. Stanchu, A.V. Kuchuk, V.P. Kladko, A.E. Belyaev, V.F. Machulin
V. Lashkaryov Institute of Semiconductor Physics, National Academy of Sciences of Ukraine,
41, prospect Nauky, 03028 Kyiv; e-mail: n.safriuk@gmail.com

Abstract. Methodical approaches to the analysis of X-ray data for GaN films grown on various buffer layers and different substrates are presented in this work. Justification of dislocation structure investigation by various methods was analyzed and approaches for evaluation of deformation level and relaxation are discussed. Clarity and accuracy of obtained structure characteristics of nitride films are under discussion. Optimization methods for experimental data processing are shown. Structural properties were obtained using high resolution X-ray diffraction with two types of scans (ω and $\omega - 2\theta$) and reciprocal space maps. Microscopic nature of spatial inhomogeneities in these structures (deformations and dislocation density) and influence of the buffer layer thickness on properties of GaN layer were discussed with account of obtained results.

Keywords: X-ray diffraction, deformations, dislocation structure, GaN layer.

Manuscript received 21.05.13; revised version received 10.07.13; accepted for publication 19.09.13; published online 30.09.13.

1. Introduction

Materials based on GaN cause a great interest due to their straight and wide band gap, high drift velocity of electrons and good physical and chemical properties [1]. They have a potential to create on their base high-performance, high-frequency electronic and optical devices, for example light emitting and laser diodes [2, 3]. Mainly, III-nitrides are grown on Al_2O_3 substrates. But Si substrate is the promising one for growing III-nitrides due to their low cost, big area, high thermal conductivity and easy integration in electronics. Nevertheless, when the thickness of GaN layer exceeds 1 µm, it starts to crack, which is caused by residual stresses generated by the lattice thermal expansion mismatch between the layer and substrate [4, 5].

The main source of defects in an epitaxial GaN layer is misfit strain relaxation caused by the lattice mismatch between the layer and substrate. Thus, the defect structure is more homogenous with great anisotropy of strain fields and appearance of explicit directions along the surface and along the surface normal. The main defects are dislocations that can be separated as misfit dislocations, i.e. localized on heteroboundaries, and threading dislocations. The latter ones are mainly generated at a growing epitaxial layer with a great mismatch between lattice parameters and the substrate ones ($\Delta a/a > 0.01$) [6].

Basicaly, analysis of an epitaxial layer is performed using the mosaic model of crystals (Fig. 1) developed in the works [7, 8]. The layer is assumed to consist of single crystallites called mosaic blocks with certain mean vertical and lateral dimensions called vertical and lateral correlation lengths, since the crystallites coherently scatter X-rays. The terms vertical and lateral relate to the directions perpendicular and parallel to the growth plane, respectively, which can be described in terms of the two crystallographic parameters: the angle of tilt that crystallites have with respect to the surface normal (out-of-plane rotation) and their range of twist around the surface normal (in-plane rotation) [9].

© 2013, V. Lashkaryov Institute of Semiconductor Physics, National Academy of Sciences of Ukraine

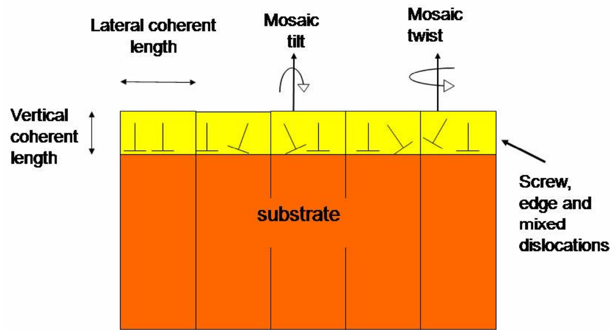

Fig. 1. Mosaic model parameters.

The main effect of dislocations on diffraction curves is broadening the diffraction peaks. At present, there are observed such effects as: broadening of asymmetric reflection curves, which is a consequence of mosaic block twists; broadening of symmetric reflection curves which is related to the average mosaic block tilt in the diffraction plane and the effective lateral size of these blocks; broadening along the diffraction vector, which is related to the strain inside mosaic blocks and their effective size in the direction normal to the surface. Separation of the two above mentioned effects can be made using the Williamson-Hall plot with account of several orders of reflection [10].

Average values of twist and tilt angles are related with the full width at the half maximum (FWHM) of diffraction peaks [11, 12]. Densities of different type dislocations correlated with FWHM and were calculated using twist and tilt angles [13].

The diffraction curves in the works [14, 15] do not have a clear Gaussian shape. They are approximated by the Voigt function with a high degree of the Lorentzian component at different scan modes. Analysis of these broadenings show that for the Bragg peaks, the Gaussian component dominates, and for the Laue peaks, the contribution of the Gaussian and Lorentzian components are practically the same. According to the authors arguments, ordered distribution of dislocations of the same type leads to the Gaussian shape of diffraction peak broadening, while chaotic distribution of dislocations leads to the Lorentzian shape. Taking into account that threading screw dislocations make the main contribution to broadening the Bragg diffraction curves (perpendicular to the diffraction vector), only horizontal dislocations make a contribution to broadening the Laue diffraction curves. Thus, one can conclude that distribution of horizontal dislocations or their components is more chaotic as compared to the distribution of vertical dislocations.

Important structural characteristics of a hexagonal GaN layer grown on the *c*-plane of sapphire can be precisely determined using the nondestructive method of high resolution X-ray diffraction. At the same time, there is a problem of an unambiguous definition and interpretation of experimental data. Performed in this work was a comparative structure analysis of GaN layer (~1 μm) grown on Si(111) and *c*-Al_2O_3 substrates by molecular beam epitaxy (MBE) with AlN layer of different thickness and AlN/GaN superlattice (SL) as buffers to determine optimal characteristics of this structure. Using high resolution X-ray diffractometry, the symmetric and asymmetric diffraction scans as well as a reciprocal space map (RSM) were obtained. Using the methods described in [10], such parameters of GaN layer were obtained, namely: (1) deformation; (2) edge and screw dislocation density; (3) tilts, twists and sizes of mosaic blocks.

2. Experiment

We studied an epitaxial GaN layer grown by MBE on Si(111) and c-Al_2O_3 substrates. The thickness of GaN layer in all our samples is ~1 μm. To improve properties of GaN layers, we used buffer layers. The samples A and C on Si(111) substrate have a buffer layer AlN with thicknesses 60 and 100 nm, respectively. The sample B and № 1 on the Si(111) and Al_2O_3(0001) substrates, respectively, contained a modulated buffer layer consisted of 5-period SL AlN/GaN.

The measurements were performed using the diffractometer “PANalytical X’Pert PRO MRD”. We used diffraction scans and RSMs of symmetric reflections from planes parallel to the surface and of asymmetric reflections from planes inclined against the surface. Azimuthal φ-scanning for asymmetric (11-2*l*) reflections was used to measure misorientation of GaN blocks with respect to the substrate plane and determine the twist angle of mosaic blocks.

3. Results

3.1. Analysis of diffraction curves from GaN films

In the work [16], it was shown that growth of nitrides on sapphire substrate is accompanied by twist of a GaN unit cell with respect to a sapphire unit cell at certain angles to reduce lattice mismatch. The same twists were observed in [17] for GaN layer on Si substrates.

To find the twist angles between a unit cell of the layer and substrate, the azimuthal φ-scanning was performed. From these measurements, it was found that for both substrates (Si and Al_2O_3), GaN unit cells grow twisted at the angles close to 30° in the direction [110] of sapphire and [112] of silicon.

It is well known that defects in GaN layer cause significant broadening both symmetric and asymmetric scans. Comparisonof rocking curves from the sample on sapphire substrate (№ 1) and on Si(111) substrate (C) for symmetric 002 and asymmetric 105 reflections are shown in Figs 2a and 2b, respectively.

The values of FWHM for both reflections and all the samples are summarized in Table 1.

© 2013, V. Lashkaryov Institute of Semiconductor Physics, National Academy of Sciences of Ukraine

Table 1. Parameters of the mosaic structure for GaN layers.

Sample	α_{tilt}, deg.	$N_S \cdot 10^9$ cm^{-2} (DCS)	$L_{\parallel}$, nm	$L_{\perp}$, nm	FWHM (002), deg.	FWHM (105), deg.
1	0.19	0.94	6500	1139	0.21	0.11
A	0.267	1.86	389	951	0.32	0.12
C	0.24	1.5	1027	836	0.29	0.18
B	0.275	1.97	1379	541	0.27	0.16

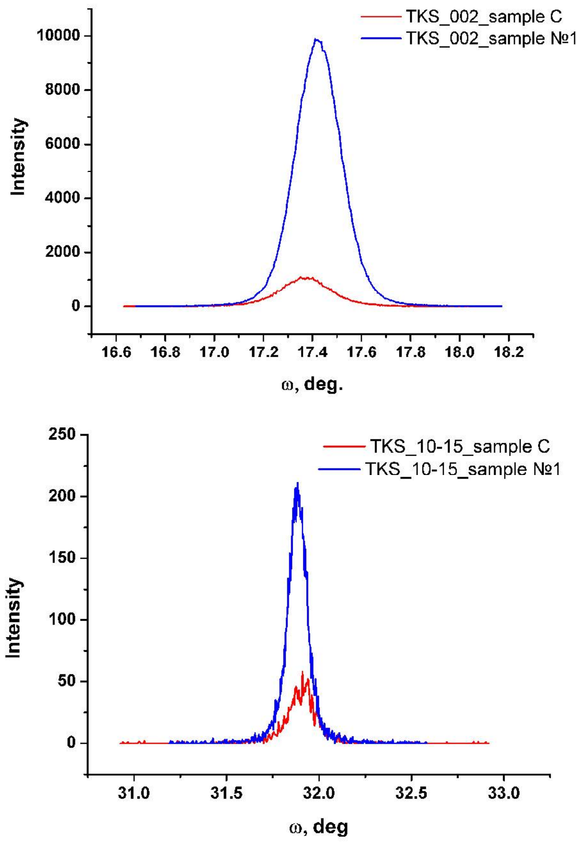

Fig. 2. Diffraction curves from GaN layer on Si and Al_2O_3 substrates, symmetric (002) (a), asymmetric (105) reflection (b).

Further, to more precisely determine FWHM and peak positions, the Pseudo-Voigt approximation function (1) was used:

$$PV(x) = (1 - f)G(x) + f \cdot L(x), \qquad (1)$$

where $G(x)$ is the Gaussian function, $L(x)$ – Lorentzian function, f – fraction $L(x)$ in the Pseudo-Voigt approximation function.

3.2. Determination of the lattice parameters from rocking curves and RSM

Williamson-Hall analysis for investigation of epitaxial structures was recently carried out, when epitaxial layers with a large mismatch and high density of structural defects were under investigation [17]. Moreover, this method was also spread on lateral intensity distribution (perpendicular to the diffraction vector).

The measurements of symmetric ω and asymmetric $\omega - 2\theta$ diffraction curves give a possibility to determine such parameters as: size of mosaic blocks in both directions – vertical ($L_{\perp}$) and parallel ($L_{\parallel}$) to the surface, average tilt angle $\langle\alpha_{tilt}\rangle$ and average deformation $\langle\varepsilon\rangle$ along the *c*-axes of GaN layer. The contribution of each parameter in the shape of a reciprocal lattice node is schematically depicted in Fig. 3.

For symmetric Bragg reflection (the reciprocal lattice vector is parallel to the surface), the parameters $\langle L_{\perp}\rangle$ and $\langle\varepsilon\rangle$ lead to broadening the reciprocal lattice node along the diffraction vector $\boldsymbol{H}$ with the values $\delta q_z = 1/\langle L_{\perp}\rangle$ and $\delta q_z = 2H\langle\varepsilon\rangle$, respectively. The lateral size and average tilt of blocks broaden intensity distribution perpendicularly to the diffraction vector direction, $\delta q_x = 1/\langle L_{\parallel}\rangle$ and $\delta q_x = 2H\langle\alpha_{tilt}\rangle$.

3.3. Tilt and twist of mosaic blocks in GaN

Broadening the diffraction peaks occurs in two directions – parallel to the diffraction vector ($\omega - 2\theta$-scan) and perpendicular to it (ω-scan) and consists of two components. FWHM of $\omega - 2\theta$-scan is given by the formula:

$$w^n = \left(\frac{\lambda}{2\langle L_{\perp}\rangle\cos\theta}\right)^n + \left(2\langle\varepsilon\rangle\tan\theta\right)^n, \qquad (2)$$

where λ is the X-ray wavelength ($\lambda_{CuK\alpha} = 0.15406$ nm); θ – diffraction angle.

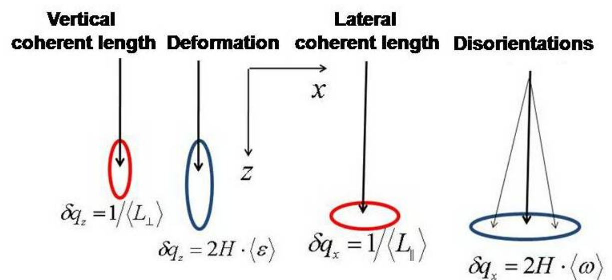

Fig. 3. Schematic broadening of a reciprocal lattice node for symmetric reflection.

© 2013, V. Lashkaryov Institute of Semiconductor Physics, National Academy of Sciences of Ukraine

Peak broadening of ω-scan is:

$$w^n = \left(\frac{\lambda}{2\langle L_{||} \rangle \sin\theta} \right)^n + \langle \alpha_{tilt} \rangle^n . \quad (3)$$

Only the first equation is used for classic polycrystal analysis. We can separate them taking into account independence of the two components from the Bragg angle. From the intersection of linear dependences of $(w \cdot \cos\theta/\lambda)^n$ on $\sin^n\theta/\lambda$, in the first case, and $(w \cdot \sin\theta/\lambda)^n$ on $\sin^n\theta/\lambda$ in the second case, using the reflections of several orders, we can obtain values of effective sizes of blocks, and from the angle of inclination of these dependences, we can obtain the values of $\langle\varepsilon\rangle$ and $\langle\alpha_{tilt}\rangle$, respectively. Different works use the linear or quadratic law of summing in Eqs (2) and (3), i.e $n = 1, 2$. The first is valid for a sum of two Lorentzian distributions, the second – for a sum of two Gaussian distributions. Eqs (2) and (3) can be approximated using the Pseudo-Voigt function with the mean n value between 1 and 2, depending on correlation between the Lorentzian and Gaussian contributions.

It is well known that in ω-mode scan, only tilts and lateral size influence on FWHM of symmetric reflection curves. Therefore, the total FWHM is given as (4):

$$\beta = \frac{0.9\lambda}{2L\sin\theta} + \alpha_{tilt} , \quad (4)$$

where L – lateral coherent length; α_{tilt} – mosaic block tilt; λ – X-ray wavelength ($\lambda_{\text{CuK}\alpha}$ = 0.15406 nm); θ – diffraction angle.

Rewriting equation (4) as

$$\beta \frac{\sin\theta}{\lambda} = \frac{0.9}{2L} + \alpha_{tilt} \frac{\sin\theta}{\lambda} , \quad (5)$$

then, by plotting β·sin(θ)/λ as a function of sin(θ)/λ for several consecutive reflections (002, 004, 006) and an approximate plot by a strain line, one can separate the contribution of tilts and sizes of mosaic blocks in broadening the diffraction curves (Fig. 4). The tilt angle α_{tilt} that is used for determination of the screw dislocation density obtained from the slope of the Williamson-Hall plot with respect to the x-axis and lateral size can be obtained from intersection of the plot with the y-axis [18].

The block tilt to the surface normal α_{tilt} arises due to the presence of dislocations with the Burgers vector $\vec{b}_s$ = [001] (for our structures $|b_s|$ = 0.5185 nm). The dislocation density can be estimated using Eq. (6):

$$N_S = \frac{\alpha_{tilt}^2}{4.35 \cdot \vec{b}_s^2} , \quad (6)$$

Full analysis of the deformation state and relaxation level of epitaxial structures can be made using the measurement of RSM. The typical shape of RSM for relaxed epitaxial structures with dislocations is ellipse. These ellipses elongate in the direction perpendicular to the diffraction vector **H** (along the axis q_x) in symmetrical Bragg geometry.

The measurement of RSM for asymmetric Bragg diffraction gives us more information about a strain state of the structures. First of all, one can obtain the level of relaxation by using asymmetric RSM. In the case when the system layer-substrate isn't relaxed, the nodes of a reciprocal lattice for the layer H_1 and substrate H_0 are located on the axis q_x (along the surface normal).

If the system layer-substrate is fully relaxed, the nodes H_1 and H_0 lay in the line q_h that is parallel to the vector of a reciprocal lattice. In general, in the case of partly relaxed structures, the node H_1 is located in the sector created by the axes q_z and q_h with their centre in H_0 (Fig. 5).

But in some cases, due to thermal stresses, the reciprocal lattice nodes can move outside the sector. As at growth temperatures (much higher than the room temperature), the film starts to relax (the position of the node H_1 located in the line q_h), and after cooling, thermal stress is generated as caused by the mismatch between the coefficients of thermal expansion of the layer and substrate. Moreover, the node H_1 can shift inside the sector or move beyond it, depending on the sign of differences between thermal expansion coefficients.

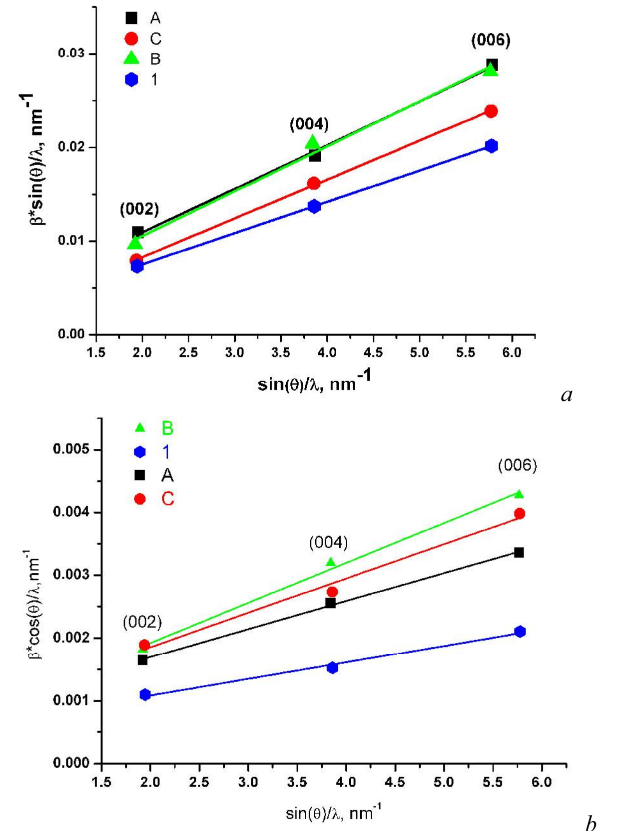

Fig. 4. Williamson-Hall plot for reflections (00*l*): a) ω-scan, b) ω–2θ-scan.

© 2013, V. Lashkaryov Institute of Semiconductor Physics, National Academy of Sciences of Ukraine

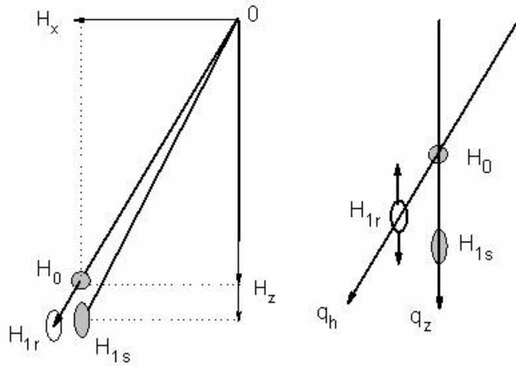

Fig. 5. Positions of the reciprocal lattice nodes on substrate (H_0), and epitaxial layer (H_{1S}) in a strain state (H_{1S}) and in a relaxed state (H_{1R}).

The measurements of a wide reciprocal space area of symmetric reflection 0002 were carried out to determine the deformation state and relaxation level for all the layers of the system: peaks of GaN layer, AlN buffer layer and substrate (Fig. 6).

Also, we have obtained RSM of asymmetric reflection 105 from GaN layer (Fig. 7). The lattice parameters *a* and *c* of GaN were calculated using both symmetric and asymmetric RSM. Lateral macrodeformation $\varepsilon_{||}$ in the growth plane was obtained from asymmetric RSM of 105 reflection.

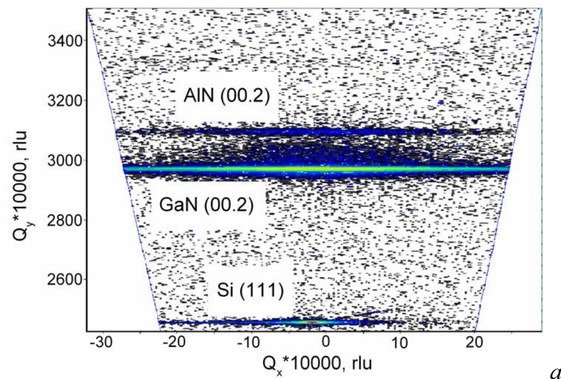

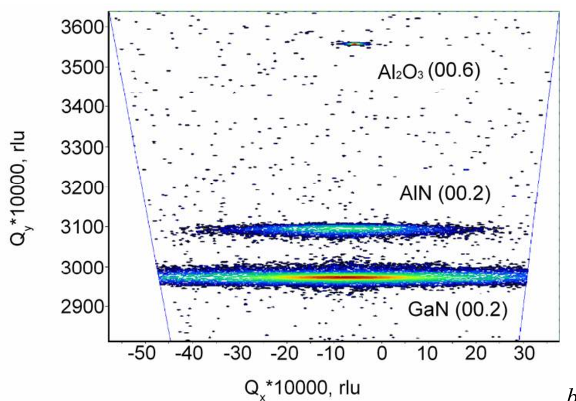

Fig. 6. Symmetric RSM of 002 reflection on Si (a) (sample C) and Al_2O_3 (sample № 1) (b) substrates.

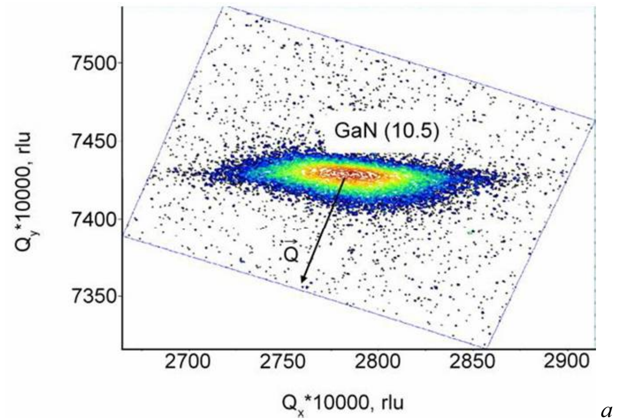

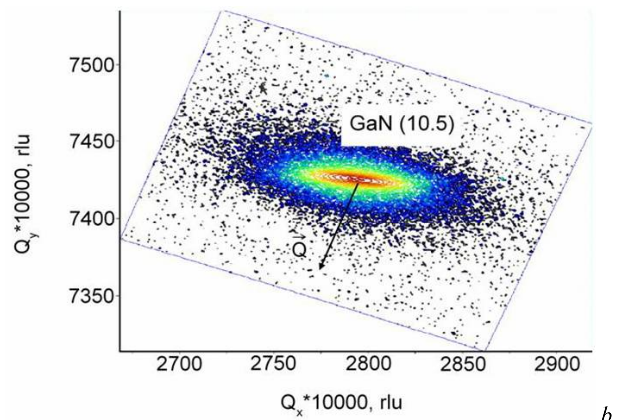

Fig. 7. Asymmetric RSM of 105 reflection on Si (sample C) (a) and Al_2O_3 (sample (№ 1) (b) substrates.

As one can see from Fig. 6, the shapes of RSM are different for structures grown on different substrates. In case of growth on Si(111) substrate, RSM elongates in the direction perpendicular to the growth direction. In the case of growth on Al_2O_3(001), elongation of RSM is observed in both directions parallel and perpendicular to the growth direction. This intensity distribution on RSM is typical of relaxed structures with the presence of mismatch dislocations. Different shapes of RSM indicate different dislocation structures. In the case of GaN-AlN-Si system, there were vertical threading dislocations of the screw and edge types. In the case of GaN-AlN-Al_2O_3 system, most likely, the share of horizontal dislocations sharply increases, and the share of vertical dislocations decreases. Thus, from the relative position of reciprocal lattice nodes and their shape, we can get information about the relaxation level of layers and dominant system of dislocations.

The influence of dislocation networks on Bragg diffraction illustrates expansion of RSM in the direction perpendicular to the diffraction vector $\vec{Q}$. This effect is shown for all the epitaxial structures. But the presence of dislocation grids doesn't lead to expansion of RSM in the direction parallel to the diffraction vector. One of the numerous methods of determinating the tilt angle was proposed in [19]. This method is based on analysis of

© 2013, V. Lashkaryov Institute of Semiconductor Physics, National Academy of Sciences of Ukraine

FWHM of asymmetric reflections at different inclination angles to the surface. The plotted curve FWHM(φ) is extrapolated to φ = 90° (method I), which is depicted on Fig. 8.

Tilt and twist angles were assumed to be independent. They depend only on the lattice plane inclination angles. FWHM, according to this approach, is defined as:

$$W(\varphi)=\left[W_{eff}^{twist}(\varphi)^n+W_{eff}^{tilt}(\varphi)^n\right]^{\frac{1}{n}}. \quad (7)$$

Here, $n=1+(1-f)^2$, $W_{eff}^{twist}(\varphi)$ and $W_{eff}^{tilt}(\varphi)$ are FWHM related to tilt and twist of mosaic blocks.

$$W_{eff}^{twist}(\varphi)=W_0^{twist}(\varphi)\exp\left(-m\frac{W_0^{tilt}(\varphi)}{W_0^{tilt}(0)}\right), \quad (8)$$

$$W_{eff}^{tilt}(\varphi)=W_0^{tilt}(\varphi)\exp\left(-m\frac{W_0^{twist}(\varphi)}{W_0^{twist}(90)}\right), \quad (9)$$

$$W_0^{twist}(\varphi)=\cos^{-1}\left(\cos^2(\varphi)\cos(W_y)+\sin^2(\varphi)\right), \quad (10)$$

$$W_0^{tilt}(\varphi)=\cos^{-1}\left(\sin^2(\varphi)\cos(\alpha_{twist})+\cos^2(\varphi)\right), \quad (11)$$

where W_y is FWHM at $\varphi=0$, W_z – FWHM at $\varphi=90°$, m – parameter that depends on the sample thickness.

The mosaic twist can be determined by finding and substituting the independent variables m and W_z in the above described equations. This twist equals to FWHM at φ = 90°.

Another method uses a combination of ω- and φ-scans of asymmetric reflections (method II). Graphically, this method is depicted in Fig. 9.

The main point of this method is that increasing the inclination angle between the crystallographic planes of asymmetric reflections and the surface leads to increasing FWHM of ω-scans, otherwise, FWHM of φ-scans decreases, and the intersection of these curves FWHM(φ) gives the value of the twist angle.

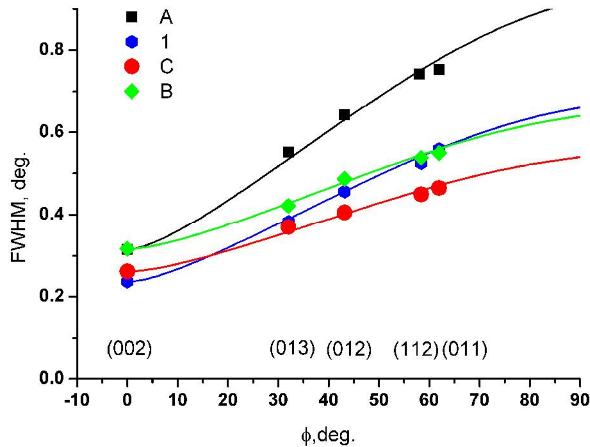

Fig. 8. Schematic determination of mosaic block twist (method I).

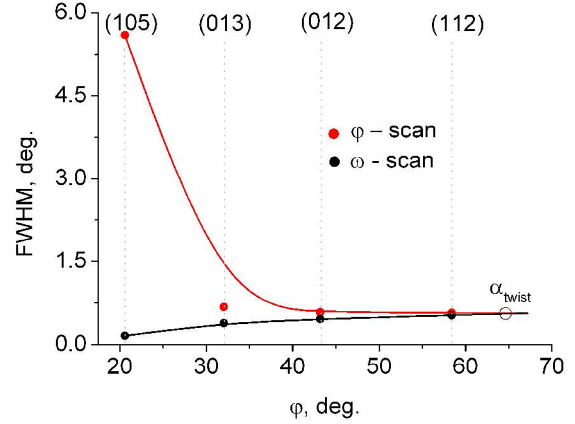

Fig. 9. Schematic determination of mosaic block twist (method II).

Calculation of the twist angles α_{twist} was performed using the equations proposed in [20] for both schemes of measurements: triple-crystal (TCS) and double-crystal ones (DCS). The values of the twist angles obtained by the method II are lower than those obtained by the method I (Table 2). The density of edge dislocations with the Burgers vectors $\mathbf{b}_E$ = 1/3⟨1120⟩ (|b_E| = 0.3189 nm) in the slip planes {1-100} leads to the mosaic block twist angles α_{twist}, which is shown with Eq. (12):

$$N_E=\frac{\alpha_{twist}^2}{4.35\cdot b_E^2}, \quad (12)$$

The edge dislocation densities obtained at different schemes and by various methods are presented in Table 2.

As one can see from Table 2, the results obtained using different methods are in good correlation. Also, it is obvious that the density of edge dislocations decreases with the increase of buffer layer thickness (for both methods). GaN layers grown on AlN/Si(111) template with the buffer thickness 100 nm have the lowest dislocation density.

Table 2. Mosaic block twist angles and density of edge dislocations in GaN layers obtained using both methods.

Sample	method I				method II	
	α_{twist}, deg. (DCS)	α_{twist}, deg. (TCS)	$N_E \cdot 10^{10}$ cm^{-2} (DCS)	$N_E \cdot 10^{10}$ cm^{-2} (TCS)	α_{twist}, deg. (DCS)	$N_E \cdot 10^{10}$ cm^{-2} (DCS)
1	0.66	0.64	3.0	2.82	0.56	2.16
A	0.91	0.83	5.7	4.74	0.69	3.28
B	0.54	0.41	2.01	1.16	0.55	2.08
C	0.64	0.6	2.82	2.48	0.63	2.73

© 2013, V. Lashkaryov Institute of Semiconductor Physics, National Academy of Sciences of Ukraine

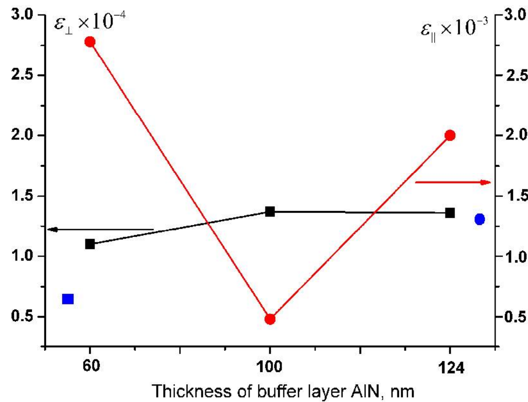

Fig. 10. Behavior of deformation in growth plane and perpendicular to it grown on Si substrate with increasing of buffer layer thickness. Values of deformations on sapphire substrate (blue dots).

Analyzing the Williamson-Hall plot and FWHM of symmetric and asymmetric reflections, it becomes clear that the sizes of mosaic blocks are bigger for GaN layers grown on Al_2O_3 substrate in comparison to those grown on Si (111) substrate. For GaN layers grown on Si substrate, we observe the increase in the lateral coherent length and decrease in the vertical coherent length with increasing the buffer thickness.

A comparison of the diffraction curves intensities obtained from all the samples shows that the intensity of curves of 0002 reflection increases with increasing the buffer thickness. The tendency of FWHM to reduce for both symmetric 002 and asymmetric 10-15 reflections was observed. The lowest FWHM and highest intensity were observed for the layer grown on sapphire substrate. Presented in Fig. 10 is behavior of deformation in the growth plane and perpendicular to it.

As one can see from Fig. 10, deformation in the growth direction $\varepsilon_\perp$ slowly increases with increasing the buffer thickness, deformation in the growth plane $\varepsilon_{||}$ has its minimum for GaN layer grown on AlN/Si(111) template with buffer thickness 100 nm. Taking into account this fact, it can be concluded that the optimal thickness of AlN buffer layer on Si(111) substrate is 100 nm. Deformations in GaN layer grown on sapphire substrate (blue dots) are smaller in the growth direction.

4. Conclusion

Hence, information about the relaxation level of the layers and the dominant system of dislocations has been obtained on the basis of the analysis of the relative position of the reciprocal lattice nodes of epitaxial layers and shape of nodes. The edge dislocations parallel to the interface contribute to broadening the symmetric Bragg reflections, while screw the dislocations parallel to the interface do not contribute. As for the edge dislocations perpendicular to the interface, they lead to broadening in skew-symmetric and grazing-incidence geometry and do not affect the symmetric Bragg reflections. Whereas, screw dislocations perpendicular to the interface affect only broadening the ω-scan of symmetric reflections.

The decrease of the screw dislocations density and increase of the lateral correlation length at increasing buffer layer thickness were observed. It was also established the decrease in the vertical correlation length and increase of deformation in the growth direction.

It was revealed that the edge dislocation density decreases with the increasing buffer layer thickness. The value of strain in the growth plane decreases with increasing buffer layer thickness. The optimal thickness of AlN buffer layer proved to be 100 nm.

Thus, the use of different schemes of diffraction, analysis of FWHM, different intensities and shapes of rocking curves and reciprocal space maps gave a possibility to find three types of dislocations, their densities and levels of relaxation in these epitaxial layers. Good correlation of the results of different methods proved the adequacy of the selected model for calculation of parameters and experimental schemes.

Acknowledgment

This paper was supported by the National Academy of Sciences of Ukraine within the framework of the scientific-technological program “Nanotechnology and Nanomaterials”.

References

1. S.C. Jain, M. Willander, J. Narayan and R. Van Overstraeten, III–nitrides: Growth, characterization, and properties // *J. Appl. Phys.* **87**(3), p. 965 (2000); A. Asgari, M. Kalafi, L. Faraone, The effects of GaN capping layer thickness on two-dimensional electron mobility in GaN/AlGaN/GaN heterostructures // *Physica E: Low-dimensional Systems and Nanostructures*, **25**(4), p. 431-437 (2005).
2. S. Fernández, F.B. Naranjo, F. Calle, E. Calleja, A. Trampert, K.H. Ploog, Growth and characterization of high-quality 10-period AlGaN/GaN Bragg reflectors grown by molecular beam epitaxy // *Mater. Sci. and Eng.: B*, **93**(1–3), p. 31-34 (2002).
3. V.P. Kladko, A.F. Kolomys, M.V. Slobodian, V.V. Strelchuk, V.G. Raycheva, A.E. Belyaev, S.S. Bukalov, H. Hardtdegen, V.A. Sydoruk, N. Klein, and S.A. Vitusevich, Internal strains and crystal structure of the layers in AlGaN/GaN heterostructures grown on sapphire substrate” // *J. Appl. Phys.* **105**(6), Article ID 063515 (2009).
4. Kai Cheng, M. Leys, S. Degroote, B. Van Daele et al., Flat GaN epitaxial layers grown on Si(111) by metalorganic vapor phase epitaxy using step-graded AlGaN intermediate layers // *J. Electron. Mater.* **35**(4), p. 592-598 (2006).

© 2013, V. Lashkaryov Institute of Semiconductor Physics, National Academy of Sciences of Ukraine

5. H. Morkoc, *Handbook of Nitride Semiconductors and Devices: GaN-based Optical and Electronic Devices.* Wiley-VCH, Berlin, 2008.
6. R.N. Kyutt, V.V. Ratnikov, G.N. Mosina, M.P. Shcheglov, Structural perfection of GaN epitaxial layers according to X-ray diffraction measurements // *Phys. Solid State,* **41**(1), p. 25-31 (1999).
7. R.N. Kyutt, A.A. Dyshekov, Effect of epilayer microstructure on shape of X-ray diffraction peaks // *Techn. Phys. Lett.* **37**(4), p. 306-308 (2011).
8. B. Liu, R. Zhang, Z.L. Xie et al., Microstructure and dislocation of epitaxial InN films revealed by high resolution X-ray diffraction // *Appl. Phys. Lett.* **103**, 023504 (2008).
9. G.K. Williamson, W.H. Hall, X-ray line broadening from filed aluminium and wolfram // *Acta Metallurgica,* **1**(1), p. 22-31 (1953).
10. V. M. Kaganer, O. Brandt, A. Trampert, K.H. Ploog, X-ray diffraction peak profiles from threading dislocations in GaN epitaxial films // *Phys. Rev. B,* **72**(4), Article ID 045423 (2005).
11. V.M. Kaganer, K.K. Sabelfeld, X-ray diffraction peaks from partially ordered misfit dislocations // *Phys. Rev. B,* **80**(18), 184105 (2009).
12. Y.J. Sun, O. Brandt, T.Y. Liu, A. Trampert, K.H. Ploog, Determination of the azimuthal orientational spread of GaN films by X-ray diffraction // *Appl. Phys. Lett.* **81**(26), p. 4928 (2002).
13. H. Heinke, V. Kirchner, S. Einfeldt, A. Hommel, X-ray diffraction analysis of the defect structure in epitaxial GaN // *Appl. Phys. Lett.* **77**(14), p. 2145 (2000).
14. R. Chierchia, T. Bottcher, H. Heinke, S. Einfeldt, S. Figge, and D. Hommel, Microstructure of heteroepitaxial GaN revealed by X-ray diffraction // *J. Appl. Phys.* **93**(11), p. 8918 (2003).
15. V.P. Kladko, A.V. Kuchuk, N.V. Safryuk, V.F. Machulin, A.E. Belyaev, H. Hardtdegen, S.A. Vitusevich, Mechanism of strain relaxation by twisted nanocolumns revealed in AlGaN/GaN heterostructures // *Appl. Phys. Lett.* **95**(3), Article ID 031907 (2009).
16. A. Dadgar, F. Schulze, M. Wienecke, A. Gadanecz, J. Bläsing, P. Veit, T. Hempel, A. Diez, J. Christen and A. Krost, Epitaxy of GaN on silicon – impact of symmetry and surface reconstruction // *New J. Phys.* **9**, p. 389 (2007).
17. M.K. Ozturk, Yu. Hongbo, B. Sarıkavak, S. Korcak, S. Ozcelik, E. Ozbay, Structural analysis of an InGaN/GaN based light emitting diode by X-ray diffraction // *J. Mater. Sci.: Mater. Electron.* **21**, p. 185-191 (2010).
18. M.A. Moram and M.E. Vickers, X-ray diffraction of III-nitrides // *Repts. Progr. Phys.* **72**(3), Article ID 036502 (2009).
19. V. Srikant, J.S. Speck, D.R. Clarke, Mosaic structure in epitaxial thin films having large lattice mismatch // *J. Appl. Phys.* **82**(9), p. 4286 (1997).
20. T. Metzger, R. Hopler, E. Born et al., Defect structure of epitaxial GaN films determined by transmission electron microscopy and triple-axis X-ray diffractometry // *Philos. Mag. A*., **77**(4), p. 1013-1025 (1998).

© 2013, V. Lashkaryov Institute of Semiconductor Physics, National Academy of Sciences of Ukraine